# Inhibition of CCL28/CCR10-Mediated eNOS Downregulation Improves Skin Wound Healing in the Obesity-Induced Mouse Model of Type 2 Diabetes

Zhenlong Chen,[1] Jacob M. Haus,[2] Lin Chen,[3,4] Ying Jiang,[5] Maria Sverdlov,[6] Luisa A. DiPietro,[3,4] Na Xiong,[7] Stephanie C. Wu,[8] Timothy J. Koh,[4,9] and Richard D. Minshall[1,5]

*Diabetes 2022;71:2166–2180 | https://doi.org/10.2337/db21-1108*

**Chronic, nonhealing skin wounds, such as diabetic foot ulcers (DFUs), are common in patients with type 2 diabetes. Here, we investigated the role of chemokine (C-C motif) ligand 28 (CCL28) and its receptor C-C chemokine receptor type 10 (CCR10) in downregulation of endothelial nitric (NO) oxide synthase (eNOS) in association with delayed skin wound healing in the *db/db* mouse model of type 2 diabetes. We observed reduced eNOS expression and elevated CCL28/CCR10 levels in dorsal skin of *db/db* mice and subdermal leg biopsy specimens from human subjects with type 2 diabetes. Further interrogation revealed that overexpression of CCR10 reduced eNOS expression, NO bioavailability, and tube formation of human dermal microvascular endothelial cells (HDMVECs) in vitro, which was recapitulated in mouse dorsal skin. In addition, incubation of HDMVECs with CCL28 led to internalization of the CCR10/eNOS complex and colocalization with lysosome-associated membrane protein 1. Finally, topical application of myristoylated CCR10 binding domain 7 amino acid (Myr-CBD7) peptide prevented CCR10-eNOS interaction and subsequent eNOS downregulation, enhanced eNOS/NO levels, eNOS/VEGF-R2$^{+}$ microvessel density, and blood perfusion, reduced inflammatory cytokine levels, and importantly, decreased wound healing time in *db/db* mice. Thus, endothelial cell CCR10 activation in genetically obese mice with type 2 diabetes promotes eNOS depletion and endothelial dysfunction, and targeted disruption of CCR10/eNOS interaction improves wound healing.**

Vascular complications of type 2 diabetes greatly reduce quality of life and likely underlie the 34% lifetime risk of developing diabetic foot ulcers (DFUs), which precede amputation in up to 84% of cases (1,2). Patients with DFUs, which are associated with a 42% mortality within 5 years, were also found to have 2.5-fold increased risk of death compared with patients with diabetes without foot ulcers (3). The underlying causes of DFUs are multifactorial, with impaired perfusion and chronic inflammation important contributors (4). Diabetes and chronic inflammation are also known to be associated with endothelial dysfunction and defective endothelial nitric oxide (NO) synthase (eNOS)-NO signaling that in turn result in defective neovascularization and wound healing (5,6). Diabetic mouse wounds exhibit reduced or unproductive angiogenesis and significantly fewer vessels despite the presence of proangiogenic factors (7). In

[1]Department of Anesthesiology, University of Illinois at Chicago, Chicago, IL
[2]School of Kinesiology, University of Michigan, Ann Arbor, MI
[3]Department of Periodontics, University of Illinois at Chicago, Chicago, IL
[4]Center for Wound Healing and Tissue Regeneration, University of Illinois at Chicago, Chicago, IL
[5]Department of Pharmacology and Regenerative Medicine, University of Illinois at Chicago, Chicago, IL
[6]Research Resources Center, Research Histology and Tissue Imaging Collaborative, University of Illinois at Chicago, Chicago, IL
[7]Department of Microbiology, Immunology and Molecular Genetics, University of Texas Health Science Center at San Antonio, San Antonio, TX
[8]Departments of Surgery and Stem Cell and Regenerative Medicine, Center for Lower Extremity Ambulatory Research, Dr. William M. Scholl College of Podiatric Medicine, Rosalind Franklin University of Medicine and Science, North Chicago, IL
[9]Department of Kinesiology and Nutrition, University of Illinois at Chicago, Chicago, IL

Corresponding authors: Richard D. Minshall, rminsh@uic.edu, and Zhenlong Chen, zlchen0305@gmail.com

Received 17 December 2021 and accepted 21 July 2022

This article contains supplementary material online at https://doi.org/10.2337/figshare.20360037.

addition, impaired wound healing and angiogenesis defects have been observed in eNOS-deficient mice (8). However, the underlying mechanisms of eNOS downregulation in peripheral microvascular endothelial cells (ECs) in type 2 diabetes and whether these can be targeted therapeutically for treatment of type 2 diabetes–related syndromes associated with peripheral vascular disease, such as DFUs, remain to be elucidated.

Defective wound healing in the mouse model of diet-induced obesity (DIO) was overcome by increasing NO production via overexpression of eNOS (9). Acarbose, a widely used oral glucose-lowering drug prescribed exclusively for patients with type 2 diabetes, increased NO production and exhibited the potential to promote wound healing and improve angiogenesis in diabetic *db/db* mice (10). Matrix metalloproteinase 2 (MMP-2) activity, hydroxyproline content, and wound breaking strength were significantly increased by the NO donor molsidomine, which partially reversed impaired wound healing in diabetic rats (11). Further, a statin-loaded tissue-engineered scaffold, which promotes eNOS expression and NO synthesis, accelerated vascularization, blood supply to wounds, and decreased wound healing time in a rat model of diabetes (12). Finally, we know that persistent inflammation is a critical factor in the chronicity of DFUs (13,14) and that eNOS-derived NO inhibits nuclear factor-κB activity and thereby can reduce inflammation in animal models (15–17). While these studies demonstrate the essential role of NO in neovascularization and wound closure, they do not provide a permanent solution due to limited bioavailability, oxidant buffering mechanisms, and desensitization of NO targets that ultimately negate the long-term effects of NO donors. Rather, we reasoned that if we could define the etiology of obesity and type 2 diabetes–linked eNOS downregulation in the peripheral microcirculation, curative prevention or treatment strategies for nonhealing skin wounds such as DFUs, which focus on restoring eNOS expression and NO bioavailability, may be possible.

Chemokine (C-C motif) ligand 28 (CCL28) was discovered in 1994 as a ligand for C-C chemokine receptor type 10 (CCR10) (18,19). CCL28 is typically secreted from epithelial cells, such as in the gut, lung, breast, and salivary gland (20). Mucosa-specific CCL28 was reported to have a predominant role in oral wound healing by increasing human gingiva fibroblast proliferation, migration, and secretion of interleukin (IL) 6 and hepatocyte growth factor (21). Facciabene et al. (22) showed that CCL28 facilitates hypoxia-induced homing of regulatory T cells that foster tumor angiogenesis by accentuating vascular endothelial (VE) growth factor (VEGF) production. CCR10 has been shown to be expressed in primary human dermal fibroblasts and microvascular ECs, and in wound-infiltrating ECs in injured BALB/c mice, suggesting the involvement of CCR10 in cutaneous wound healing (23). Furthermore, Chen et al. (24) reported that stimulation of human myeloid cells and ECs with lipopolysaccharide, IL-1β, IL-6, IL-17, and tumor necrosis factor-α (TNF-α) increased the expression of CCL28 and CCR10 mRNA.

Recently, we demonstrated that chemokine receptor CCR10, which is highly expressed in human ECs, mediates ligand CCL28-dependent EC migration (24), directly binds to eNOS, and inhibits eNOS activity (25). Here we assessed the hypothesis that upregulation of chemokine CCL28 in type 2 diabetes and resultant persistent activation of its primary receptor CCR10 in dermal microvascular ECs leads to eNOS downregulation via a lysosomal degradation pathway. We thus assessed levels of CCL28 in plasma and subdermal biopsy specimens from patients with type 2 diabetes and spontaneous (leptin receptor mutant, $Lepr^{db}$) diabetic animals, as well as tissue levels of CCL28, CCR10, and eNOS in the context of type 2 diabetes and associated vascular dysfunction. In addition, we hypothesized that topical application of a myristoylated 7 amino acid CCR10 binding domain peptide (Myr-CBD7) (25) to full-thickness mouse dorsal skin wounds would block EC CCR10-eNOS interaction in the *db/db* mouse, prevent or reverse eNOS downregulation, and restore NO levels and wound angiogenesis while simultaneously reducing proinflammatory cytokine levels and wound healing time. This study thus tests the idea that targeting a protein-protein interaction uniquely responsible for eNOS downregulation in type 2 diabetes may be an effective future strategy for treating DFUs.

## RESEARCH DESIGN AND METHODS

### Human Subjects

Participants were recruited from the Chicago, IL, metropolitan area, and all subjects were screened via health history, medical examination, resting electrocardiogram, and fasting blood chemistry in the University of Illinois at Chicago Clinical Research Center. Full experimental procedures have been presented previously (26–28). Briefly, two groups of participants were recruited, a type 2 diabetes group ($n$ = 8) and a lean healthy control (LHC) group ($n$ = 10). Following an ~12 h overnight fast, serum and plasma blood samples (antecubital vein) and subdermal needle biopsy specimens of the vastus lateralis were obtained under local anesthetic (lidocaine HCl 2%) using a 5 mm Bergstrom cannula with suction. Tissue was blotted, trimmed of adipose and connective tissue if necessary, and processed according to assay. All studies were approved by the University of Illinois at Chicago Institutional Review Boards and performed in accordance with the Declaration of Helsinki. Written informed consent was obtained from all research participants during the initial screening visit.

### Mouse Healing Models

All animal procedures were performed in accordance with the Guide for the Care and Use of Laboratory Animals (National Institutes of Health). Wild-type (WT; C57BL/6J) and $eNOS^{-/-}$ mice were purchased from Jackson Laboratory (Bar Harbor, ME). $CCR10^{-/-}$ mice were generated

in Dr. Na Xiong's laboratory (UT San Antonio). Depending on the duration and goal of each study, four 5-mm or two 8-mm full-thickness excisional wounds were made on the dorsal skin of male mice (9 weeks old) using a standard skin biopsy punch (Acuderm, Fort Lauderdale, FL) under ketamine (100 mg/kg) and xylazine (5 mg/kg) anesthesia. Myristoylated (Myr-) scrambled control peptide (Myr-Ctl-P) or Myr-CBD7 peptides (25) were applied topically to wounds in F-127 Pluronic gel (25% gel in saline; Sigma-Aldrich, St Louis, MO) right after wounding (29). Wound size was determined as previously described (25,30), and wound tissues were collected at indicated times for biochemical or histological analysis.

### Reagents

F-127 Pluronic gel, dithiothreitol, BSA, and radioimmunoprecipitation assay (RIPA) buffer were from Sigma-Aldrich (St. Louis, MO). *n*-Octyl-β-*D*-glucopyranoside (ODG) was from RPI Corp (Mt Prospect, IL). TransIT transfection reagent was from Mirus Bio (Madison, WI). Mouse anti-CCR10 and mouse anti-eNOS antibodies were from Santa Cruz Biotechnology (Dallas, TX). Lipofectamine 2000, DMEM, DAPI, fluorescently labeled secondary antibodies, TRIzol, and SYBR Green PCR mix were from Thermo Fisher Scientific (Waltham, MA). Mouse anti-eNOS and mouse anti-actin antibodies, human recombinant CCL28, and Matrigel matrix were from BD Biosciences (San Diego, CA). Rabbit anti-EEA1 and VEGF-R2, mouse anti–lysosome-associated membrane protein 1 (LAMP1), and eNOS antibodies, rabbit monoclonal anti-CD31, and Griess Reagent kit were from Cell Signaling Technology (Danvers, MA). Nitrocellulose membrane was from Bio-Rad Laboratories (Hercules, CA). SuperSignal West Femto Kit and Restore Western Stripping buffer were from Pierce (Rockford, IL). The skin punch biopsy tool was from Acuderm (Fort Lauderdale, FL). Mouse ELISA kits were purchased from R&D Systems (Minneapolis, MN).

### Construction of CCR10-GFP Plasmid

To generate the WT, C-terminal green fluorescent protein (GFP)–tagged C-C motif in CCR10, full-length *Homo sapiens* CCR10 cDNA (Addgene, Cambridge, MA) was used as a DNA template in a PCR reaction with DNA Phusion High-Fidelity Polymerase (New England BioLabs, Ipswich, MA). The following primer pair lacking the stop codon was used: CCR10-ATG-*Eco*RI-F: 5′- AAAAAA**GAATTC**ATGGGGACGG AGGCCACAGAG-3′ and CCR10-NoStop-*Kpn*I-R: 5′- AAAA AA**GGTACC**AAGTTGTCCCAGGAGAGACTGTG-3′. The resultant PCR fragment was digested with restriction enzymes 5′-*Eco*RI and 3′-*Kpn*I (italicized and underlined in the primers) and ligated using T4 DNA Ligase (New England BioLabs) into pEGFP-N1 vector (Clontech, Mountain View, CA) digested with the same restriction enzymes. The ligated reaction was transformed into Subcloning Efficient DH5α Competent Cells (Thermo Fisher Scientific).

### Cell Culture and Transfection

Human dermal microvascular ECs (HDMVECs) were purchased from Cell Biologics (Chicago, IL). EC growth medium (EGM-2 plus Bullet kit) was from Lonza (Walkersville, MD). HEK 293 cells were from the ATCC (Rockville, MD) and were cultured in DMEM supplemented with 10% FBS and 1% penicillin/streptomycin. Transfection of CCR10-GFP cDNA in ECs was by TransIT and in HEK cells by Lipofectamine 2000, as described previously (24,25,28). Cells transduced with fluorescently tagged proteins were verified by fluorescence microscopy and immunoblot analysis.

### Overexpression of CCR10 with Adenovirus CCR10 in Dorsal Skin of WT Mice

After WT C57BL/6 mice (9 weeks old) were shaved, 100 μL adenovirus (Adv)-CCR10 or control Adv ($1 \times 10^9$ particles/mL) was subcutaneously injected into four labeled areas of dorsal skin per mouse. Wounds (5 mm) were produced at each labeled area 3 weeks after Adv injection. Wound sizes were measured daily, as described previously (25,30), and wounds were collected on day 7 and prepared for further measurements.

### NO Measurement

Nitrite measurement of supernatants homogenates of cells or tissues was analyzed by Griess Reagent, and nitrite level was normalized to eNOS expression level in the corresponding samples as described previously (30).

### Coimmunoprecipitation and Western Blotting

For ECs, following serum starvation, control peptide or Myr-CBD7 peptide was added 45 min prior to stimulation for indicated times at 37°C, and cells were then collected and lysed with RIPA buffer (for Western blotting) or in 2% ODG in Tris buffer for coimmunoprecipitation (co-IP). For both human and mouse tissues or excised wounds, at indicated times, the dorsal skin or wounds were collected and homogenized in RIPA buffer or in 2% ODG in Tris buffer, and homogenates were then further prepared for immunoblotting or co-IP experiments, as described previously (24,30).

### EC Tube Formation

Nearly confluent HDMVECs were transfected with cDNA of human CCR10-GFP. After 48 h, the cells were transferred to 96 well plates preloaded with Matrigel matrix, and images were collected using an Olympus IX51 microscope (Olympus-Life Science, Waltham, MA), as described previously (24,25).

### Synthesis of Myr-Peptides

Myr-scrambled peptide (MSIALKS) and CBD7 (KISASLM) were synthesized as described previously (25); then, 10 mmol/L aliquots of Myr-peptides in DMSO were stored at −80°C.

### Immunohistochemistry of Dorsal Wounds

Formalin-fixed mouse skin samples were processed with an ASP300 S automated tissue processor (Leica Biosystems, Lincolnshire, IL) using a standard overnight processing protocol and embedded into paraffin blocks. For staining formalin-fixed paraffin-embedded tissue with anti-CD31 (Cell Signaling, no. 92841) rabbit monoclonal antibody (Ab), anti-eNOS mouse monoclonal Ab (BD Biosciences, no. 610297), and anti-VEGFR2 rabbit monoclonal Ab (Cell Signaling, no. 9698) to label ECs, sections (5 μm) were deparaffinized, rehydrated, and stained on a BOND RX automated stainer (Leica Biosystems) using a preset protocol. In brief, for single chromogen immunohistochemistry with CD31 Ab, sections were subjected to EDTA-based antigen retrieval (BOND ER2 solution, pH 9.0) for 20 min at 100°C. Endogenous peroxidase activity and nonspecific binding was blocked by treating samples with peroxidase block and protein block (Background Sniper; Biocare Medical, Pacheco, CA) for 15 and 30 min at room temperature, respectively. Sections were then incubated with the primary Ab diluted at 1:200 for 30 min at room temperature. BOND Polymer Refine Detection kit (Leica Biosystems) was used for detection. All sections were then counterstained with hematoxylin for 10 min and mounted with Micromount media (Leica Microsystems). Whole-slide images were acquired at ×20 magnification on an Aperio AT2 digital automated scanner (Leica Biosystems) or Zeiss LSM 880 confocal microscope, as described above. For the sequential dual immunofluorescence staining with eNOS and VEGFR2, the sections were subjected to the same antigen retrieval and then incubated with eNOS (1:75) and VEGFR2 (1:100) Abs for 1 h at room temperature, and the targets were detected with the secondary Abs conjugated with Alexa-488 (1:400; Cell Signaling, no. 4408,) and Alexa-555 (1:400; Cell Signaling, no. 4413,) correspondingly. Nuclei were stained with DAPI for 10 min at room temperature, and slides were mounted with ProLong Diamond Antifade mounting media (Thermo Fisher Scientific, no. P36961). High-power fields were scanned on Vectra Polaris (Akoya Biosciences), and images were unmixed in InForm software using the spectral library prepared from Alexa-488, Alexa-555, and DAPI monostains and a mouse skin tissue autofluorescent slide. The degree of colocalization between eNOS and VEGFR2, and vascular density represented as a percentage of total tissue area occupied by eNOS and VEGFR2 to the total area of the tissue was analyzed using QuPath image analysis software.

### Confocal Microscopy

For cellular immunostaining, confluent monolayers of cells grown on coverslips were prepared, and fluorescent images were obtained using a Zeiss LSM 880 confocal microscope, as described previously (25,28). The colocalization coefficient in specified regions of interest (ROI) was determined using Zeiss Zen software, as described previously (25). For wound tissue analysis of eNOS and VEGF-R2 immunostaining, formalin-fixed, paraffin-embedded sections were scanned at ×20 magnification with 488/555 nm laser excitation; filtered emissions were collected at 1024 × 1024 pixel resolution with pinhole set to achieve 1 Airy unit and analyzed using Zeiss Zen and ImageJ software.

### Real-Time RT-PCR

Total cellular RNA from mouse skin wounds and human tissue was extracted using TRIzol. mRNA level used to assess relative gene expression was examined by real-time RT-PCR using a SYBR Green PCR mix. All primers (listed in Supplementary Table 1) were purchased from Integrated DNA Technologies IDT (Coralville, IA). Relative gene expression was determined by the $\Delta\Delta C_t$ method based on GAPDH levels, as described previously (31,32).

### ELISA Measurement

Human tissue, mouse skin wounds, or blood serum were collected, lysed, and prepared for ELISA measurement of mouse CCL28, IL-6, TNF-α, IL-1β, and VEGF, according to the manufacturer's instructions.

### Laser Speckle Contrast Analysis

Dermal perfusion of *db/db* mouse skin wounds treated with scrambled control peptide or Myr-CBD7 peptide were analyzed on day 10 by laser speckle imager, as described previously (33,34). Blood perfusion was measured in a 100 $mm^2$ surface area, which included the excisional wound, with a PeriCam PSI System (PeriMed; resolution 0.54 × 0.54 mm, working distance 10–20 cm).

### Statistical Analysis

Data are expressed as mean ± SD. Statistical analysis was performed using Prism 9.1.0 (GraphPad Software, San Diego, CA). Comparison between two groups was by unpaired, two-tailed *t* test with Welch correction for unequal SDs. Comparison among three or more groups was by one-way ANOVA. Comparison between two groups with multiple time points was by two-way ANOVA. In all cases, statistical significance was defined as $P < 0.05$.

### Data and Resource Availability

The resources and data sets generated during the current study are available from the corresponding author upon reasonable request.

## RESULTS

### Reduced eNOS Expression and Elevated Levels of CCL28 and CCR10 in Subdermal Tissue From Patients With Type 2 Diabetes and Full-Thickness Skin Biopsy Specimens From Genetically Obese and Diabetic *db/db* Mice

In a previous study, we showed that the plasma NO concentration is higher in the basal state in LHC subjects compared with subjects with type 2 diabetes (26). Here, we extend this observation by assessing the expression level of eNOS, an important endothelial marker protein and

indicator of peripheral vascular health (35), in human subdermal biopsy specimens. As shown in Fig. 1*A*, the protein level of eNOS was significantly lower in patients with type 2 diabetes compared with LHC subjects, consistent with previous studies (26,28).

We also recently demonstrated that chemokine receptor CCR10, which is highly expressed in human ECs, mediates ligand CCL28-dependent EC migration (24), directly binds to eNOS, and inhibits eNOS activity (25). Thus, we hypothesized that upregulation of chemokine CCL28 in type 2 diabetes and chronic activation of its primary receptor CCR10 in dermal microvascular ECs may promote eNOS downregulation. We next assessed the expression level of chemokine CCL28 and its receptor CCR10 in human biopsy specimens. CCR10 was elevated significantly in subjects with type 2 diabetes relative to LHC subjects (Fig. 1*B*; see Supplementary Table 1 for details on primers). In addition, the CCL28 level in plasma (Fig. 1*C*) and subdermal biopsy specimens was higher (Fig. 1*D*) in type 2 diabetes compared with LHC subjects. The levels of eNOS and CCR10 were also measured in diabetic *db/db* mice, which exhibited increased body weight, high blood glucose, and reduced VEGF levels in dorsal skin compared with WT mice (Supplementary Fig. 1). In dorsal skin of *db/db* mice, eNOS expression was significantly reduced (Fig. 1*E*), and CCR10 mRNA was elevated (Fig. 1*F*). Consistent with

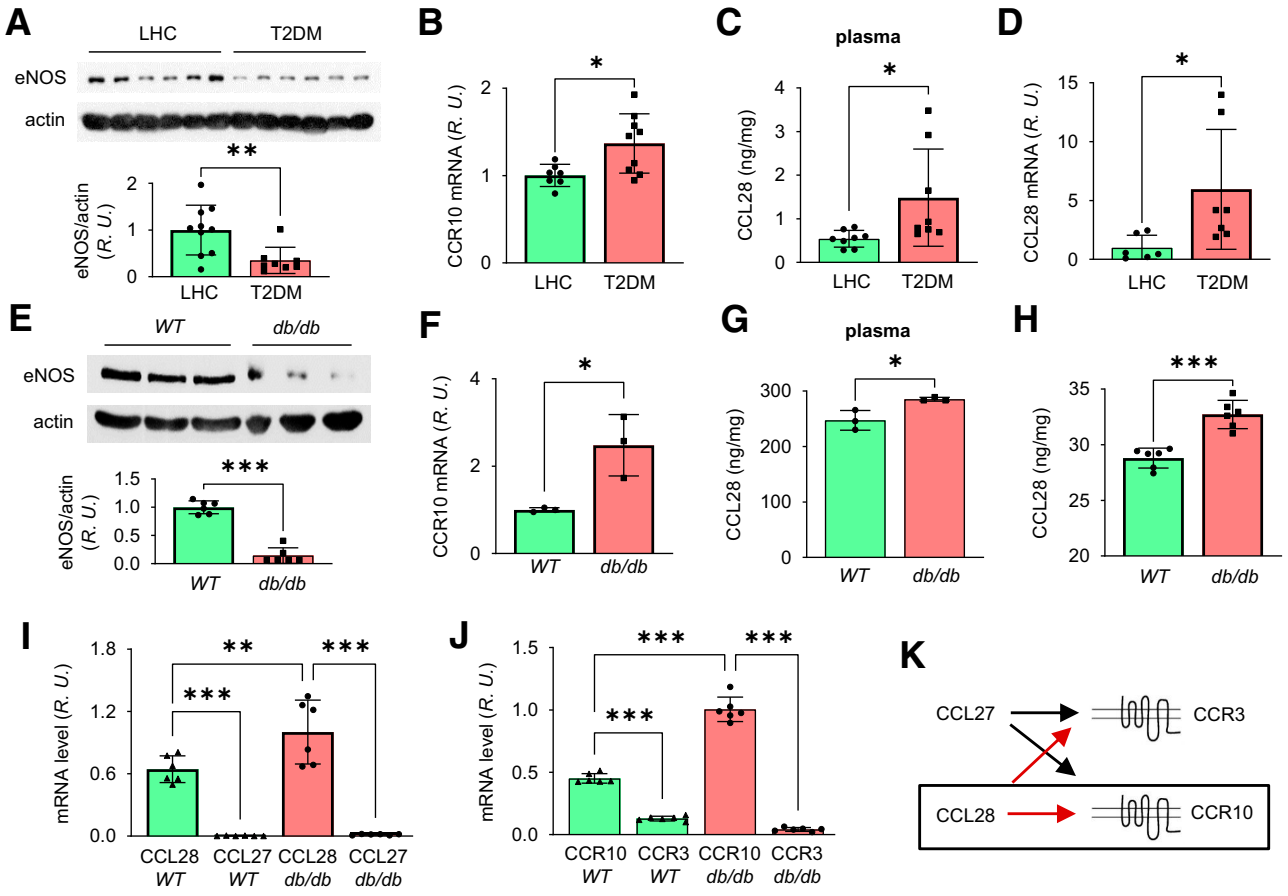


**Figure 1**—Reduced eNOS expression and elevated CCR10 level in punch biopsy specimens from human subjects and *db/db* mice with type 2 diabetes. *A*: Upper panel, subdermal biopsy specimens obtained from LHC donors and patients with type 2 diabetes were homogenized in RIPA buffer and prepared for Western blot. Bottom panel, normalized values of eNOS expression. *B*: Quantitative real-time RT-PCR revealed upregulated CCR10 mRNA in type 2 diabetes compared with LHC donors. Elevated plasma level of CCL28 determined by ELISA and mRNA by real-time RT-PCR in type 2 diabetes samples (*C*) compared with LHC (*D*). *E*: Less eNOS protein level in the dorsal skin of *db/db* mice. Mouse dorsal skin was collected and prepared for Western blotting, and normalized values are shown in the bar graph. *F*: Quantitative PCR revealed elevated CCR10 mRNA in *db/db* mouse dorsal skin compared with WT mice. Increased levels of CCL28 in plasma (*G*) and in dorsal skin (*H*) by ELISA measurement in *db/db* mice compared with WT mice. *I–K*: Comparison of mRNA levels of CCL27 and CCL28 and their receptors CCR3 and CCR10 in dorsal skin tissue of WT and *db/db* mice. *I*: Dorsal skin was collected and prepared for real-time RT-PCR. CCL28 expression level was greater than CCL27 in both WT and *db/db* mouse skin, and CCL28 expression was greater in *db/db* dorsal skin compared with WT. *J*: CCR10 expression was greater than CCR3 in both WT and *db/db* mice, while higher CCR10 mRNA level was obtained in *db/db* dorsal skin compared with WT. R.U., relative units. *K*: The signaling pair of CCL28/CCR10 (black box), rather than CCL27/CCR3, was thus chosen for further study in *db/db* mouse wound healing. Data are mean ± SD. $*P < 0.05$, $**P < 0.01$, $***P < 0.001$.

human biopsy specimens, the plasma level of CCL28 and that in dorsal skin was also significantly higher in *db/db* mice (Fig. 1*G* and *H*). Taken together, patients and mice with type 2 diabetes exhibit reduced eNOS and elevated level of CCL28/CCR10. We next determined whether CCL28 activation of CCR10 and direct interaction between CCR10 and eNOS plays a role in the downregulation of eNOS in type 2 diabetes.

Chemokines CCL27 and CCL28 can both bind to CCR3 (36) as well as CCR10 (18,37), and CCL27 and CCR3 were reported to be important in wound healing (23,38). We thus assessed their expression in dorsal skin tissue of *C57BL/6* WT and diabetic *db/db* mice by real-time RT-PCR. mRNA levels of CCL28 and CCR10 were higher than CCL27 and CCR3 in both *db/db* and WT mice (Fig. 1*I* and *J*), respectively. Thus, as CCL28/CCR10 (Fig. 1*K*) were the predominant isoforms expressed in mouse skin, they were the primary focus of all subsequent studies.

### Reciprocal Relationship Between eNOS and CCR10 Expression in Mouse Dorsal Skin

To better understand the relationship between CCR10 and eNOS, dorsal skin from *eNOS*$^{-/-}$, *db/db*, WT, and *CCR10*$^{-/-}$ mice was collected and prepared for determination of protein expression levels by Western blot. As shown in Fig. 2*A*, we observed reduced eNOS and increased CCR10 expression in *db/db* mice, and interestingly, eNOS expression was elevated in *CCR10*$^{-/-}$ mice. On the contrary, the CCR10 mRNA level in mouse skin was surprisingly elevated in *eNOS*$^{-/-}$ mice (Fig. 2*B*). Thus, whenever CCR10 expression increases, eNOS level decreases, and vice versa. These data indicate there may be a counterbalancing relationship between eNOS and CCR10 and that overexpression and activation of CCR10 via CCL28 may downregulate eNOS expression in the skin of diabetic mice.

We next verified the wound healing phenotype of the four mouse strains. Wounds were produced on the dorsal skin, and images were collected daily (Fig. 2*C*). The *db/db* mutant and *eNOS*$^{-/-}$ mouse lines showed significantly delayed wound healing compared with WT mice, and *CCR10*$^{-/-}$ mice showed only a slight delay in wound healing (Fig. 2*C* and *D*). The *db/db* mice exhibited the slowest wound healing profile, which may be partly due to high levels of proinflammatory cytokines IL-1β, IL-6, and TNF-α in the skin (Fig. 2*E*), in addition to elevated CCL28/CCR10 levels (Fig. 1*E–H*).

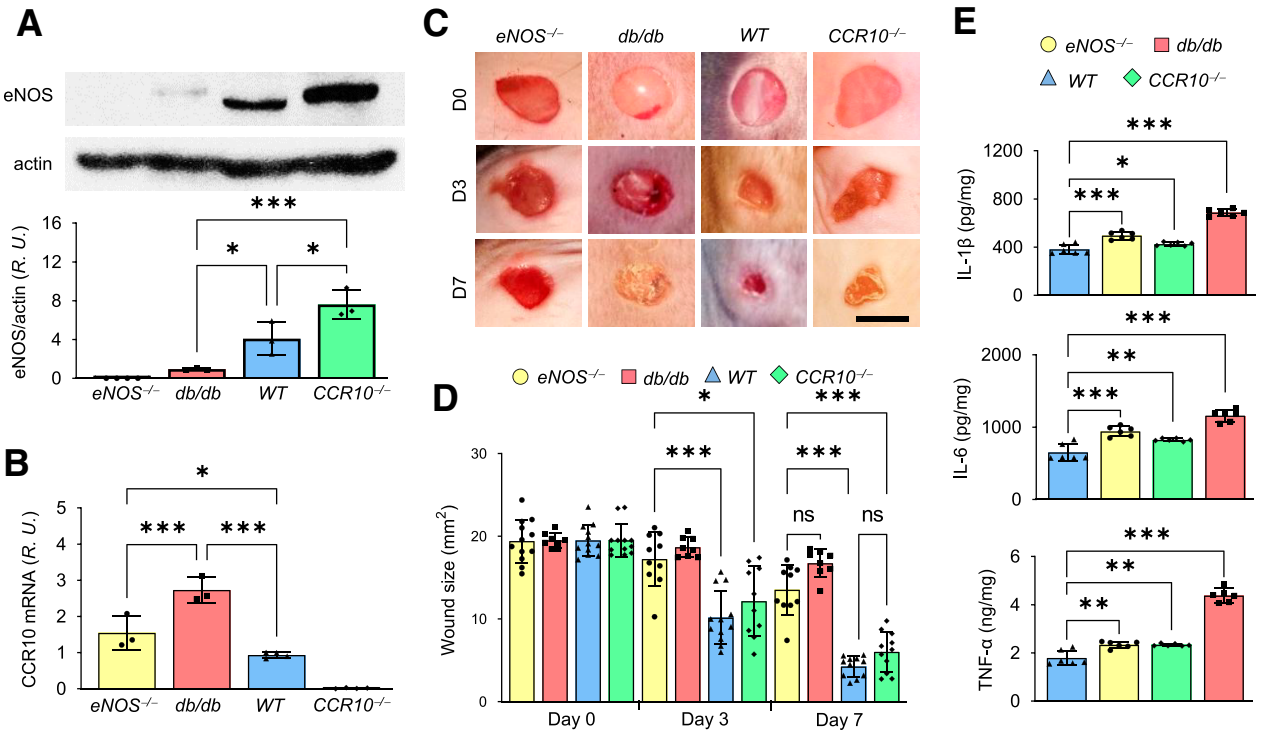


**Figure 2**—Reciprocal relationship between eNOS and CCR10 expression. *A*: Dorsal skin from *eNOS*$^{-/-}$, *db/db*, WT, and *CCR10*$^{-/-}$ mice was collected and prepared for Western blotting to detect eNOS expression; normalized values are shown in the bottom panel. *B*: mRNA level of CCR10 in dorsal skin by real-time RT-PCR. Note the expression levels of eNOS and CCR10 are opposite in mouse skin. R.U., relative units. *C*: Representative photomicrographs of wounds in WT, *CCR10*$^{-/-}$, *eNOS*$^{-/-}$, and *db/db* mice. Four 5-mm full-thickness excisional wounds were made on the mouse dorsal skin, and wound images were acquired at indicated times. D, day. Scale bar, 5 mm. *D*: Normalized wound size over time in WT, *CCR10*$^{-/-}$, *eNOS*$^{-/-}$, and *db/db* mice. *E*: Levels of proinflammatory cytokines IL-1β, IL-6, and TNF-α in dorsal skin of *CCR10*$^{-/-}$, *eNOS*$^{-/-}$, *db/db*, and WT mice were determined by ELISA. Data are presented as mean ± SD. **P* < 0.05, ***P* < 0.01, ****P* < 0.001.

### Overexpression of CCR10 Reduces eNOS Expression and Delays Wound Healing

To further assess whether the overexpression of CCR10 directly reduces eNOS expression in WT mice, we subcutaneously injected Adv-CCR10 in the dorsal skin. After 3 weeks, CCR10 mRNA was significantly elevated compared with that observed after control Adv injection (Fig. 3*A*). In addition, eNOS level was reduced (Fig. 3*B*), whereas levels of IL-1β, IL-6, TNF-α (Fig. 3*C*–*E*), and CCL28 all increased (Fig. 3*F*) in Adv-CCR10–infected mouse skin. These mice also displayed delayed skin wound healing compared with control Adv (Fig. 3*G* and *H*), indicating overexpression of CCR10 induces eNOS downregulation and inflammation, which may be causally linked to delayed wound healing.

### Overexpression of CCR10 Reduces eNOS/NO Levels and Angiogenesis in Human Dermal Microvascular ECs and HEK/eNOS Cells

We previously showed that CCR10 was highly expressed in human umbilical vein ECs (HUVECs) and human endothelial progenitor cells (24). Following stimulation with 500 ng/mL CCL28, CCR10 binding to eNOS in human dermal microvascular ECs (HDMVECs) peaked at 5 min (Fig. 4*A*), similar to that observed in HUVEC (25). Evidence of CCR10-eNOS interaction was further shown by confocal microscopy (Fig. 4*B*). Upon stimulation with CCL28 for 5 min, CCR10 (red) colocalized to a greater extent with eNOS (green) on the plasma membrane (yellow indicated by white arrows in Fig. 4*B*).

To better understand whether and how eNOS is regulated by CCR10 in dermal ECs, CCR10-GFP cDNA was transduced in primary culture HDMVECs. As shown in Fig. 4*C*, with increasing amount of CCR10-GFP cDNA transfected, eNOS expression level correspondingly was reduced, as was EC tube formation in Matrigel (Fig. 4*D*). Transduction of CCR10-GFP cDNA in stably selected eNOS-overexpressing HEK cells (HEK/eNOS) (28) also reduced eNOS expression and NO production (Fig. 4*E* and *F*). However, the reverse was not also true (i.e., overexpression of eNOS had no effect on CCR10 expression in stable HEK/CCR10-GFP cells) (Supplementary Fig. 2). Taken together, these results suggest that overexpression of CCR10 reduces eNOS expression and NO production, potentially due to direct binding to eNOS, which results in an attenuated angiogenic response.

### Prevention of eNOS Internalization With Myr-CBD7 Peptide in HDMVECs Stimulated With CCL28 With Myr-CBD7 Peptide

With persistent stimulation, G protein–coupled receptors (GPCRs) are phosphorylated by G protein receptor kinases

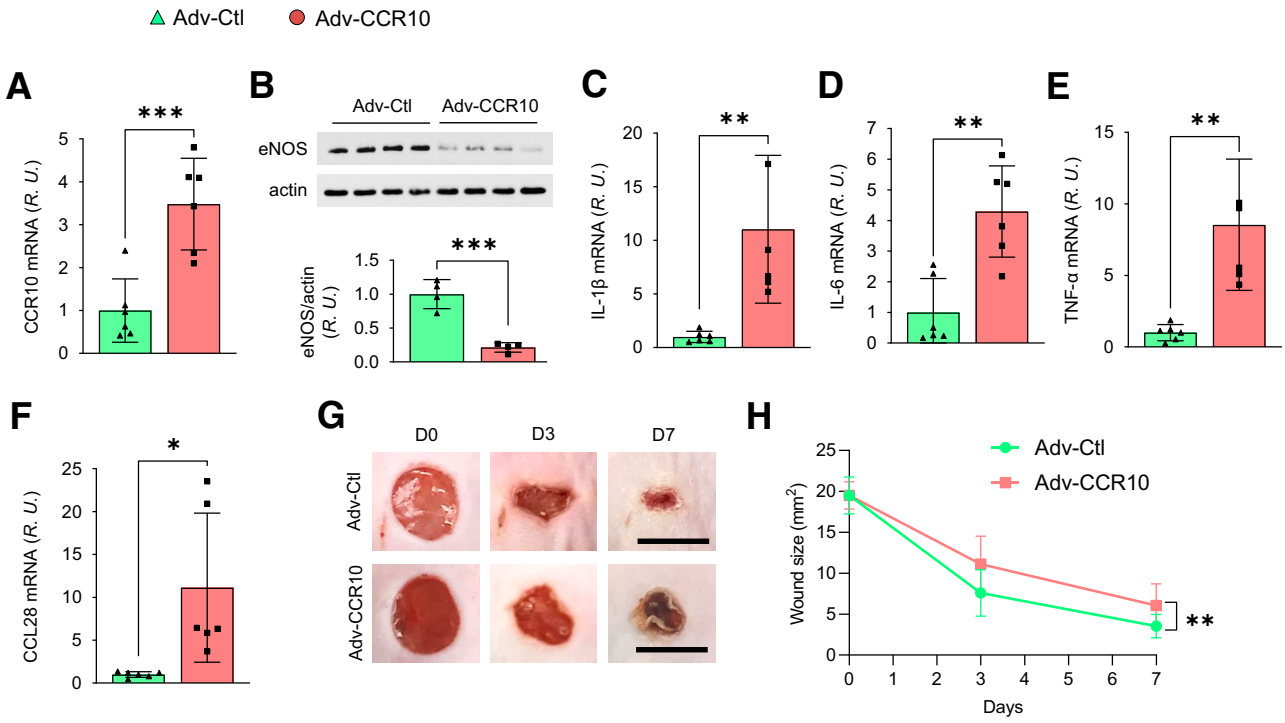


**Figure 3**—CCR10 overexpression delays dorsal skin wound healing. *A*: WT mice were injected subcutaneously in the four typical dorsal wound regions with 100 μL empty vector Adv control (Adv-Ctl) or CCR10-expressing Adv (Adv-CCR10; $1 \times 10^9$ particles/mL), and the skin was subsequently harvested and homogenized after 72 h. CCR10 mRNA, as determined by RT-PCR, was overexpressed approximately threefold above basal control level. *B*: Adv-CCR10 reduced eNOS expression in dermal microvessels. Elevated mRNA levels of IL-1β (*C*), IL-6 (*D*), TNF-α (*E*), and CCL28 (*F*) were observed in Adv-CCR10 infected mouse skin. R.U., relative units. *G* and *H*: Delayed skin wound healing was also noted in Adv-CCR10 transfected mice. Four 5 mm full-thickness excisional wounds were produced on the mouse dorsal skin, and wound images were taken at indicated times. D, day. Scale bar, 5 mm. Data are presented as mean ± SD. Average wound area of four wounds/mouse is presented as mean ± SD ($n = 6$). *$P < 0.05$, **$P < 0.01$, ***$P < 0.001$.

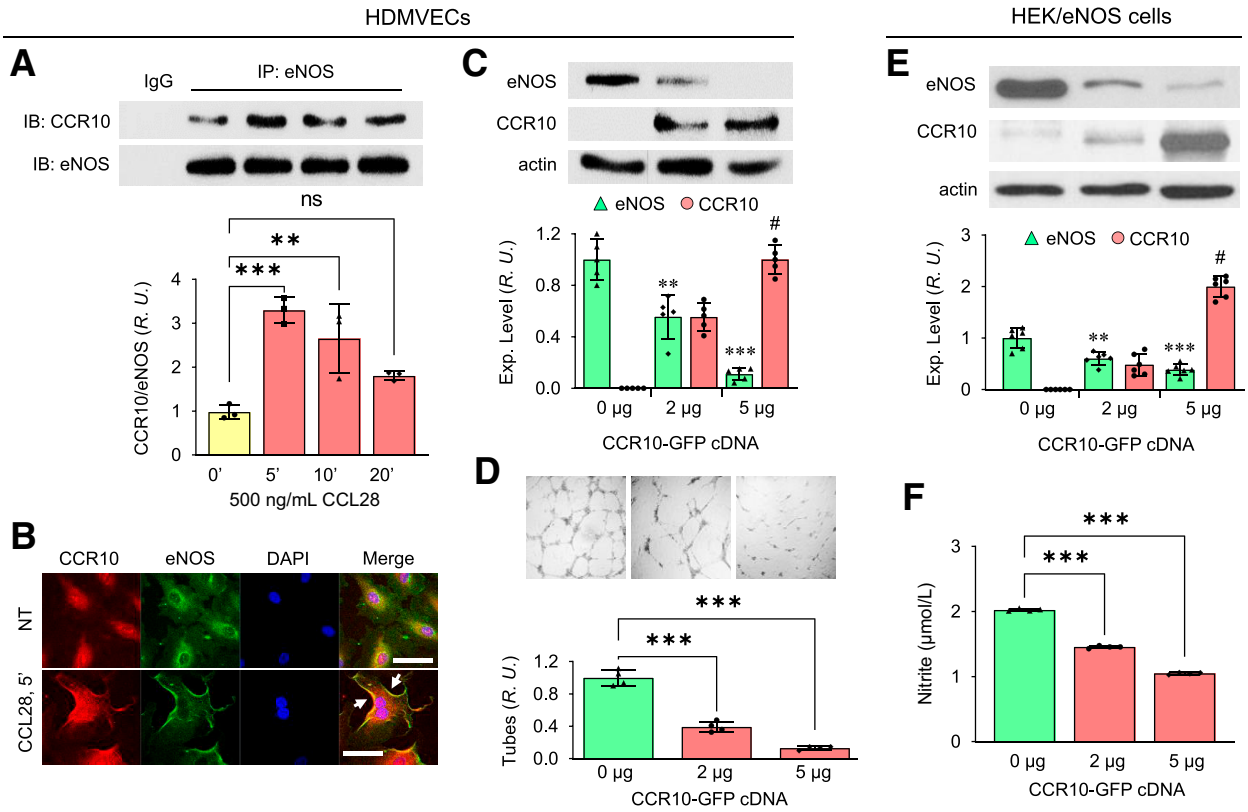


**Figure 4**—CCR10 overexpression downregulates eNOS and attenuates angiogenesis. *A*: Increased interaction between CCR10 and eNOS in HDMVECs following treatment with 500 ng/mL CCL28. After treatment, the cells were collected and immunoprecipitated (IP) with anti-eNOS Ab. Normalized ratios between CCR10 and eNOS are shown in the bottom panel. IB, immunoblot; R.U., relative units. Data are presented as mean ± SD. $*P < 0.05$, $**P < 0.01$, $***P < 0.001$ vs. time 0. *B*: Confocal microscopy reveals colocalization (white arrows) between CCR10 (red) and eNOS (green) in HDMVECs following stimulation with 500 ng/mL CCL28 for 5 min. DAPI (blue) is a nuclear marker. NT, no treatment. Scale bar, 10 μm. Similar results were observed in five independent experiments. *C*: eNOS expression in HDMVECs transduced with CCR10-GFP cDNA. Cells were collected 48 h after transfection with different amounts of CCR10-GFP cDNA and lysed for Western blotting. Normalized expression of eNOS and CCR10 are shown in the bottom panel. *D*: Angiogenesis (tube formation) of HDMVECs transfected with CCR10-GFP cDNA. Top panel, photomicrographs of EC tubes on Matrigel-coated plates 2 days after transfection in culture medium supplemented with 500 ng/mL CCL28. Bottom panel, normalized EC tube number. Data are presented as mean ± SD. $**P < 0.01$, $***P < 0.001$ vs. 0 μg CCR10-GFP; $P < 0.001$ vs. 2 μg CCR10-GFP. Reduced eNOS expression level (*E*) and NO production (*F*) in HEK/eNOS cells transduced with CCR10-GFP cDNA. Data are presented as mean ± SD. $**P < 0.01$, $***P < 0.001$ vs. 0 μg CCR10-GFP; $P < 0.001$ vs. 2 μg CCR10-GFP.

(GRKs), which leads to the recruitment of β-arrestin and receptor desensitization (39). Activated GPCRs are generally internalized via clathrin- or caveolae-mediated endocytosis and either targeted to lysosomes for degradation or dephosphorylated and recycled back to the cell surface to enable a new round of activation (39). In a preliminary study, we observed an increase in colocalization between eNOS and early endosome antigen 1 (EEA1) in HDMVECs 90 min after treatment with 500 ng/mL CCL28 (Supplementary Fig. 3), suggesting CCL28-activation of CCR10 in ECs leads to eNOS internalization.

Recently, we reported that Myr-CBD7 peptide based on the primary sequence of eNOS could block eNOS interaction with CCR10, leading to an increase in eNOS activity in HUVECs (25). Here, we tested whether Myr-CBD7 could prevent eNOS internalization and degradation in HDMVECs and determined whether this affected NO production. Confocal microscopy revealed that eNOS (green) colocalized (yellow) with LAMP1 (red) in the perinuclear region of cells pretreated with control peptide (middle panel in Fig. 5*A*). The increase in colocalization between eNOS and LAMP1 was abolished by pretreatment of Myr-CBD7 peptide in the $LAMP1^+$ ROI (Fig. 5*B*), and eNOS remained on the plasma membrane (indicated by white arrows in bottom panel of Fig. 5*A*), similar to no treatment (top panel in Fig. 5*A*). However, eNOS co-IP experiments further indicated that both eNOS and CCR10 interact with LAMP1 (Fig. 5*C–E*), suggesting that both proteins are internalized and targeted for degradation in lysosomes. However, whereas pretreatment of ECs with Myr-CBD7 reduced eNOS interaction with LAMP1 in CCL28-stimulated cells (Fig. 5*D*), it had no effect on CCR10-LAMP1 interaction, supporting the premise that Myr-CBD7 prevents eNOS binding and internalization with CCR10 leading to its degradation.

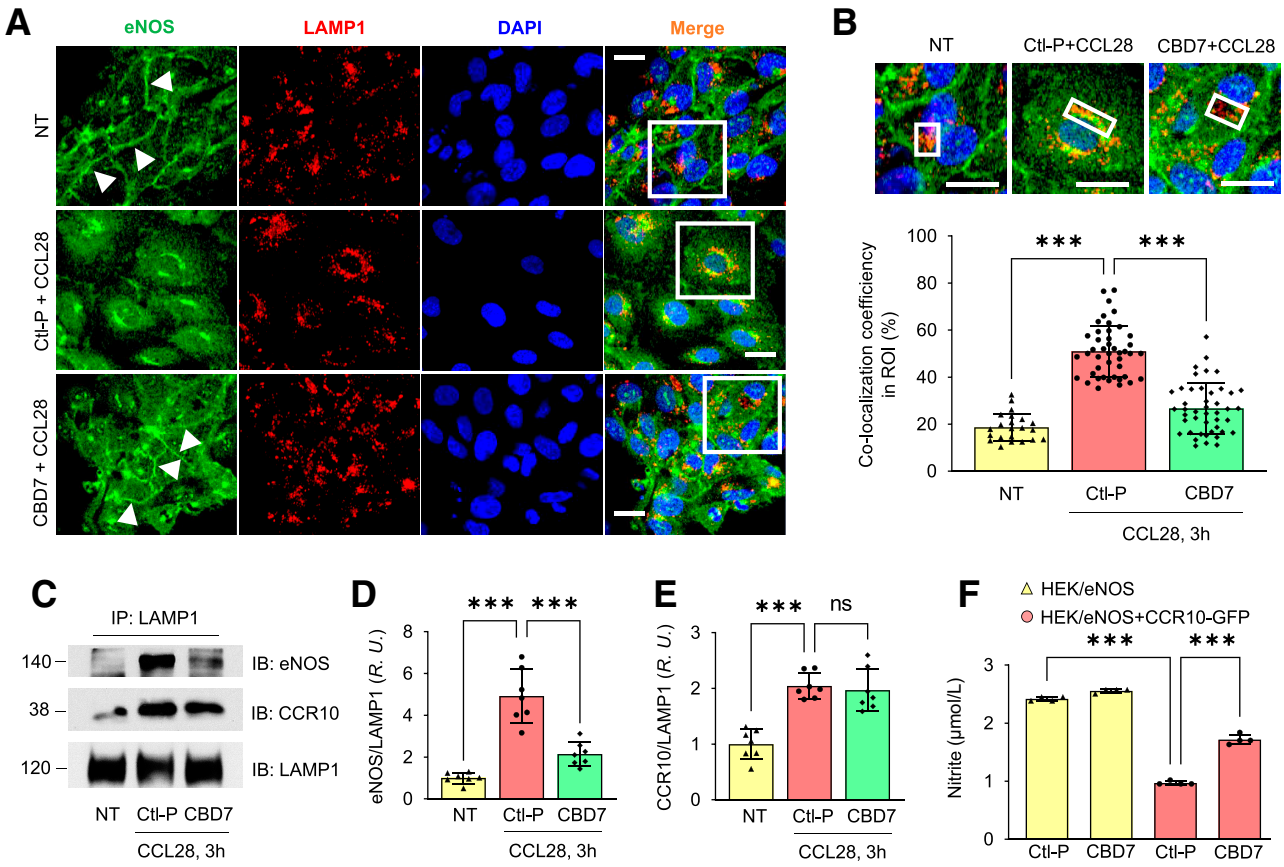


**Figure 5—**Myr-CBD7 treatment prevents eNOS degradation by blocking eNOS-LAMP1 interaction in HDMVECs stimulated with CCL28. *A*: In cells pretreated with control peptide, eNOS (green) internalization and colocalization with LAMP1 was observed following stimulation with 500 ng/mL CCL28 for 3 h (middle panel), whereas eNOS remained associated with the plasma membrane of ECs pretreated with Myr-CBD7 peptide (bottom panel), similar to no treatment (NT) (top panel). Scale bar, 10 μm. *B*: Enlarged images of white boxes in panel *A*. Bar graph: colocalization coefficient between eNOS and LAMP1 in $LAMP1^+$ ROI (white boxes). Scale bar, 10 μm. (*C*) After the same treatment as in *A*, cells were collected, and anti-LAMP1 Ab was used to immunoprecipitate (IP) cell lysates. IB, immunoblot. Normalized interaction between LAMP1 with eNOS (*D*) and CCR10 (*E*). R.U., relative units. (*F*) Effect of Myr-CBD7 peptide on NO production in HEK/eNOS cells transfected with CCR10-GFP cDNAs. After pretreatment with 50 μmol/L Myr-control or CBD7 peptide, cells were further stimulated with 5 μmol/L A23187 for 1 h at 37°C. Supernatants were assessed for total nitrite concentration. Data are presented as mean ± SD. *** $P < 0.001$.

Protein levels of the samples prior to IP (loading controls) were not different (Supplementary Fig. 4).

Furthermore, in HEK/eNOS cells transfected with CCR10-GFP, NO production was elevated significantly by pretreatment with Myr-CBD7 compared with control peptide (Fig. 5*F*). These data suggest that eNOS, due to its interaction with CCR10, is internalized and degraded following activation of ECs with CCL28. Myr-CBD7–mediated blockade of eNOS-CCR10 interaction led to reduced degradation in lysosomes, maintenance of eNOS expression and localization at the plasma membrane, and greater NO production.

### Topical Application of Myr-CBD7 to Dorsal Skin Wounds on Diabetic *db/db* Mice Enhanced eNOS/NO Levels, Microvessel Density, Blood Perfusion, and Wound Healing

Two 8-mm full-thickness excisional wounds were made on the dorsal skin of diabetic *db/db* mice, and then 50 μL of 50 μmol/L Myr-CBD7 or scrambled control peptide (Myr-Ctl-P) was topically administered. Myr-CBD7 peptide treatment significantly decreased wound healing time by 4 days (wound size on mice treated with control peptide on days 8, 10, and 12 was equivalent to Myr-CBD7 treated wounds on days 4, 6, and 8, respectively). Myr-CBD7 reduced wound size significantly starting on day 4 to a mean of 27.9% of the day 0 wound size as compared with 51.5% of the original 8 mm wounds in the Myr-Ctl-P treated group ($P < 0.001$ by two-way ANOVA for repeated measures) on day 12 (Fig. 6*A*). Both eNOS expression (Fig. 6*B*) and NO production (Fig. 6*C*) were elevated significantly in wounds on day 12 following treatment with Myr-CBD7 peptide. Furthermore, we observed reduced CCR10-eNOS interaction in mouse wounds by co-IP (Fig. 6*D*), and CD31 immunostaining of wound sections revealed enhanced microvessel density on day 12 following Myr-CBD7 treatment (Fig. 6*F*) relative to Myr-Ctl-P (Fig. 6*E*). In other experiments, day 10 skin wounds in *db/db* mice treated with Myr-CBD7 (Fig. 6*G*) exhibited a

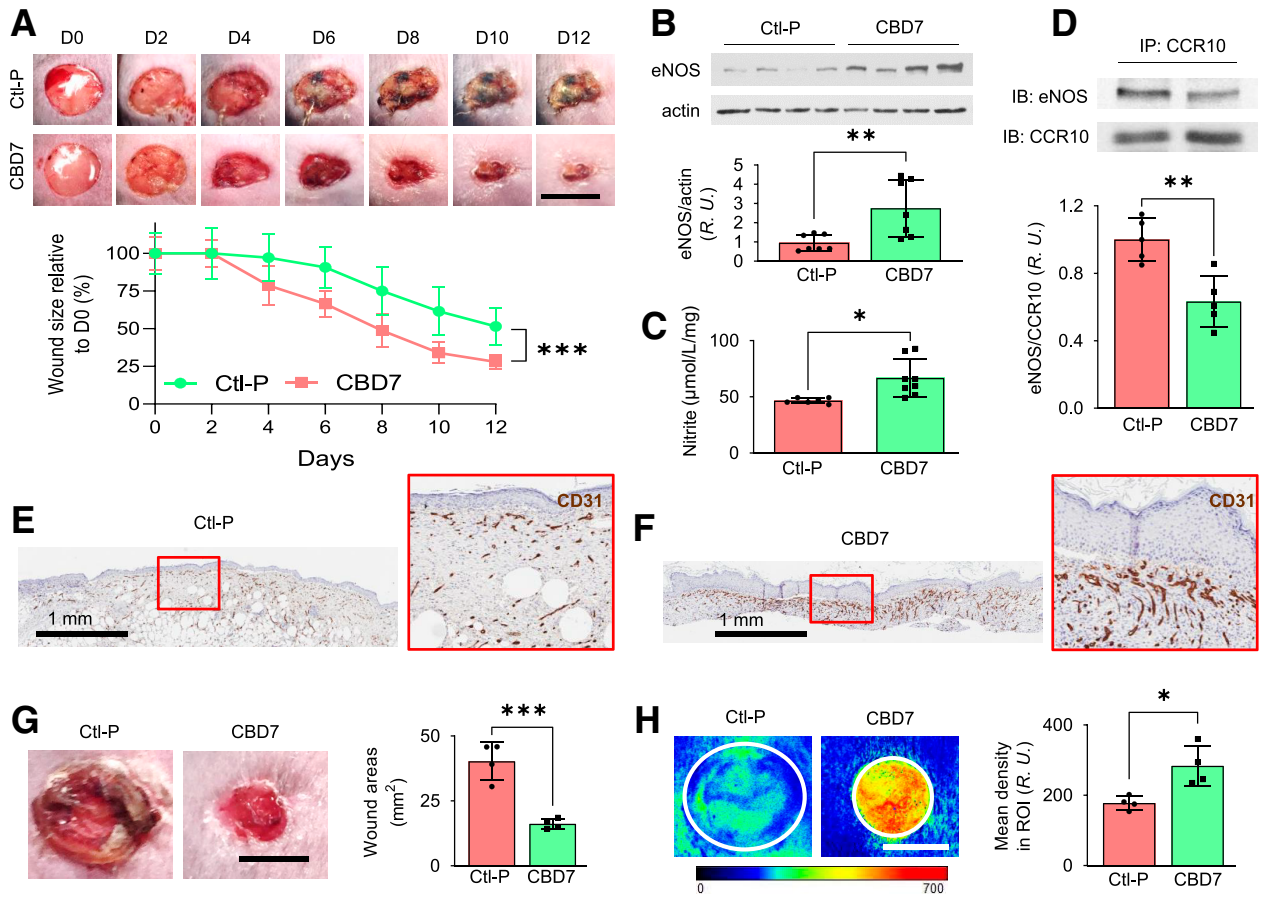


**Figure 6**—Topical application of Myr-CBD7 elevated eNOS/NO level and microvessel density in association with reduced *db/db* mouse skin wound healing time. *A*: Representative photomicrographs of 8-mm full-thickness excisional wounds after treatment with 50 μL of 50 μmol/L Ctl-P or Myr-CBD7 peptide per wound. Scale bar, 8 mm. D, day. Myr-CBD7 peptide in Pluronic solution was topically applied twice during the first 24 h after wounding, which reduced wound size significantly from day 4 onward. Myr-CBD7 increased eNOS expression (*B*) and elevated NO production (Griess reaction) (*C*) on day 12 after treating *db/db* mouse wounds with Myr-CBD7. R.U., relative units. *D*: Myr-CBD7 reduced CCR10-eNOS interaction observed by co-IP from day 12 mouse wounds compared with control peptide. IB, immunoblot. Immunohistochemical staining of CD31 (brown color) in dorsal wounds of *db/db* mice after treatment with control peptide (*E*) compared with Myr-CBD7 (*F*) on day 12 (representative of at least eight independent experiments). Blood perfusion measured by laser speckle contrast analysis (*G*) in *db/db* mouse wounds (*H*) (same wounds that are shown in panel *G*) was significantly enhanced on day 10 in mice treated with Myr-CBD7 peptide. Scale bar, 5 mm. Data are presented as mean ± SD. $*P < 0.05$, $**P < 0.01$, $***P < 0.001$.

significant increase in blood perfusion (Fig. 6*H*) detected by near-infrared laser speckle contrast analysis. These data suggest Myr-CBD7 peptide treatment prevents eNOS inhibition and internalization/degradation in association with CCR10 and that this enhances NO production, microvessel density, and blood perfusion, which contributes significantly to improving skin wound healing in obesity-induced diabetic mice.

### Alteration of Dorsal Skin Wound Microenvironment in *db/db* Mice Following Topical Administration of Myr-CBD7 Peptide

In addition to the observed increase in microvessel density and blood perfusion in *db/db* mouse wounds following treatment with Myr-CBD7 peptide, we also investigated whether topical application of Myr-CBD7 affects key inflammatory factors associated with the wound healing processes. Mouse wounds on day 3 (inflammation phase) and day 12 (proliferation and remodeling phases) were collected and prepared for determination of targeted factors by ELISA, immunohistochemistry, and real-time RT-PCR (Fig. 7).

On day 3, wounds treated initially with Myr-CBD7 peptide showed reduced CCL28 as well as proinflammatory cytokines IL-1β, IL-6, and TNF-α (M1 markers) by ELISA (Fig. 7*A–D*). In addition, mRNA levels of IL-6 and CCR10 were reduced (Supplementary Fig. 5). Interestingly, mRNA level of arginase 1 (Arg1; M2 marker) (Fig. 7*E*) increased, while transforming growth factor (TGF)-β1 (Fig. 7*F*), but not TGF-β2 (Supplementary Fig. 5) was decreased in Myr-CBD7 peptide–treated wounds.

On day 12, *db/db* mouse wounds treated with Myr-CBD7 showed an elevated level of VEGF (Fig. 7*G*), which was still lower than that observed in WT mice (Supplementary Fig. 2).

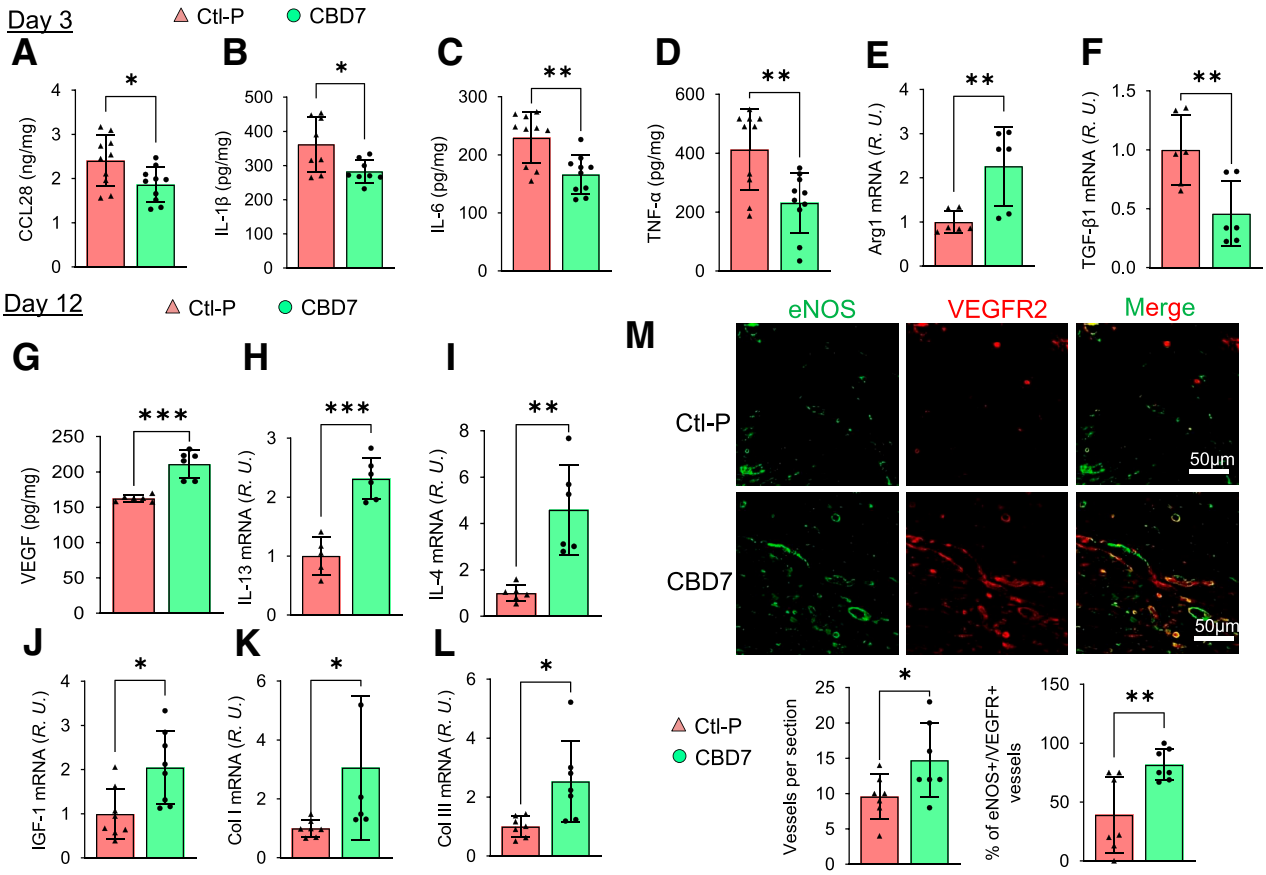


**Figure 7**—Alteration of *db/db* mouse wound microenvironment by treatment with Myr-CBD7 peptide. Skin wounds of *db/db* mice treated with 50 μmol/L Myr-CBD7 or Myr- Ctl-P were collected on day 3 or day 12 and analyzed by ELISA or RT-PCR. By day 3, Myr-CBD7 reduced the levels of CCL28 (*A*) and proinflammatory cytokines TNF-α (*B*), IL-1β (*C*), and IL-6 (*D*), increased Arg1 mRNA (*E*), and decreased TGF-β1 mRNA (*F*). R.U., relative units. By day 12, Myr-CBD7 treatment resulted in the upregulation VEGF (*G*) and anti-inflammatory cytokines IL-13 (*H*) and IL-4 (*I*) as well as IGF-1 (*J*), Col I (*K*), and Col III (*L*) genes in *db/db* mouse wounds. *M*: Fluorescent immunohistochemistry of eNOS and VEGFR2 in formaldehyde-fixed paraffin-embedded wound tissue sections following initial treatment with Myr-Ctl-P or Myr-CBD7 at day 12. Note increase in vessel density and percentage of double-positive vessels in Myr-CBD7–treated wounds. Data are mean ± SD ($n$ = 6–8). *$P < 0.05$, **$P < 0.01$, ***$P < 0.001$.

There was also an increase in the mRNA levels of anti-inflammatory cytokines IL-13 and IL-4 (M2 markers) (Fig. 7*H* and *I*), as well as insulin-like growth factor 1 (IGF-1) (Fig. 7*J*) and extracellular matrix proteins collagen I (Col I) and Col III (Fig. 7*K* and *L*). In addition, Myr-CBD7 treatment enhanced microvascular eNOS and VEGFR2 protein expression and vessel density (Fig. 7*M*) and mRNA expression of EC markers eNOS, CD31, VEGFR2, and VE-cadherin (Supplementary Fig. 5*D*–*G*). Taken together, these data suggest that blocking CCR10-eNOS interaction with Myr-CBD7 peptide upregulates eNOS/NO production and that this leads to a switch from the predominantly proinflammatory (M1) to an anti-inflammatory (M2) environment conducive of angiogenesis required for accelerating the otherwise dysfunctional diabetic skin wound healing program (Fig. 8).

## DISCUSSION

In this series of experiments, we established a novel mechanism linking excessive CCL28/CCR10 signaling to the downregulation of eNOS expression and NO production associated with inflammation, dysfunctional vasoregulation, reduced angiogenesis, and delayed skin wound healing in type 2 diabetes. First, we observed higher levels of CCL28/CCR10 and less eNOS expression in subdermal biopsy specimens from subjects with diabetes compared with LHC subjects and from the dorsal skin of diabetic mice. Next, confirming the above findings, we were able to show that overexpression of CCR10 induces the downregulation of eNOS and that this leads to *1*) reduced NO production and angiogenesis in vitro and *2*) increased inflammatory cytokine levels and delayed dorsal skin wound healing in vivo. Finally, we demonstrated using a novel peptide inhibitor of CCR10-eNOS interaction (Myr-CBD7) (25) that disruption of CCR10-mediated eNOS downregulation was sufficient to restore eNOS/NO levels, enhance angiogenesis, and decrease wound healing time in the *db/db* diabetic mice. Importantly, this innovative peptide strategy of reversing endothelial pathobiology and improving angiogenesis and skin wound healing in type 2

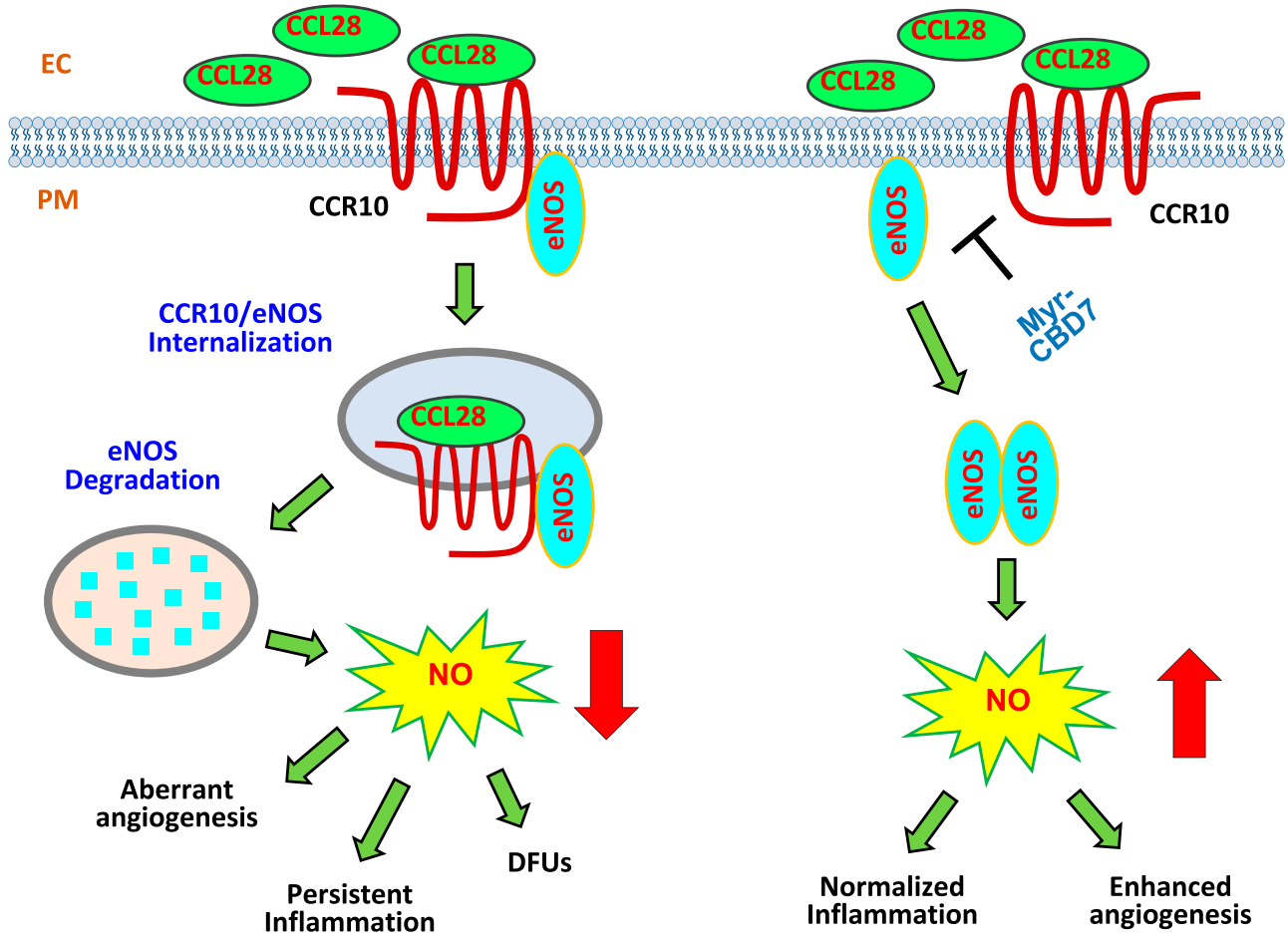


**Figure 8**—Schematic hypothesis: Excessive CCL28-dependent CCR10-mediated eNOS downregulation in dermal microvessels of subjects with type 2 diabetes. Left panel, overexpression of CCL28 activates its receptor CCR10, promoting direct binding to eNOS in ECs. eNOS is internalized together with CCR10, a GPCR, into $EEA1^+$ and $LAMP1^+$ structures where it is presumed to be degraded. Thus, the data indicate eNOS expression/NO production is reduced, leading to aberrant angiogenesis, inflammation, and delayed wound healing in type 2 diabetes. Right panel, treatment with Myr-CBD7 blocks CCR10-eNOS interaction, upregulates eNOS expression and NO production, and results in enhanced angiogenesis, normalized inflammation, and improved skin wound healing in subjects with type 2 diabetes. PM, plasma membrane.

diabetes may provide a targeted therapeutic approach for treatment of DFUs (Fig. 8).

In patients with diabetes and individuals with chronic inflammatory vascular disease/peripheral vascular disease, skin wound healing is delayed, resulting in chronic "nonhealing" wounds (40). Persistent hyperglycemia in diabetes leads to EC dysfunction, which results in decreased proangiogenic signaling and NO production (41) in both macro- and microvascular beds in animals and human subjects (42,43). A poor vasodilatory response in distal tissues results in reduced blood flow and delivery of essential cellular nutrients in DFUs (44). Decreased NO and microvascular dysfunction in DFUs also contributes to diabetic peripheral neuropathy with decreased sensation, often leading to an undetected tissue injury. Such an injury is compounded by inflammation and vascular dysfunction due to reduced eNOS/NO levels leading to slower healing, high risk for infection, and limb/nerve ischemia (43–46). Although extensive studies have established that inflammation, ischemia, and neuropathy contribute to the development of DFUs, there is a lack of knowledge of the cellular and molecular mechanisms associated with endothelial dysfunction and pathological angiogenesis that limits our ability to effectively treat DFUs (4).

Delayed wound healing observed in $eNOS^{-/-}$ mice was strikingly similar to that observed in *db/db* mice. In addition to impaired wound healing (8), $eNOS^{-/-}$ mice also exhibit abnormalities in vascular function, including insulin resistance (47). The diffusible free radical NO participates in the orchestration of wound healing and critically influences macrophage, fibroblast, and keratinocyte behavior (48,49) as well as vascular growth and remodeling during repair (50,51). The beneficial effects of NO on wound repair are attributed to the regulation of angiogenesis, inflammation, cell proliferation, matrix deposition, and remodeling (51,52). NO donor or genetic augmentation of eNOS expression in rat or human vascular smooth muscle cells enhanced vascular generation of VEGF (53,54),

one of the most potent proangiogenic agents (55). eNOS-derived NO induces *S*-nitrosylation of p65 and subsequent nuclear factor-κB inhibition (56). Topical application of the NO donor *S*-nitrosoglutathione to wounds significantly increased the mRNA expression levels of IGF-1 and accelerated wound healing in C57BL/6 mice (57). The NO donor *S*-nitroso-*N*-acetyl-penicillamine also enhanced collagen synthesis by rat dermal fibroblasts (58).

Consistent with the above findings, we observed that during the early phase (e.g., day 3) of the diabetic wounds, Myr-CBD7 peptide reduced proinflammatory cytokines IL-1β, IL-6, and TNF-α and increased the level of anti-inflammatory Arg1. At a later stage of wound healing (e.g., day 12), we observed increased levels of growth factors VEGF and IGF-1, Col I and Col III, and anti-inflammatory cytokines IL-13 and IL-4 that are essential for cell proliferation and wound healing. Importantly, the effect of Myr-CBD7, whose sequence is based on the CCR10 binding domain of eNOS (19,25), is to specifically block eNOS degradation in ECs and thereby upregulate NO bioavailability required for angiogenesis and anti-inflammatory effects. Indeed, levels of several EC markers (CD31, VEGFR2, and VE-cadherin) were elevated in addition to eNOS, most likely reflecting the increase in eNOS expression as well as EC number associated with a productive angiogenic response. While time to complete wound closure was not determined in this study, mean wound size was nearly double in diabetic wounds treated with the control peptide compared with Myr-CBD7–treated wounds on day 12. Overall, our study highlights the potential of restoring eNOS-derived NO production using an inhibitor of CCR10/eNOS protein-protein interaction, Myr-CBD7. This novel and highly targeted strategy for decreasing inflammation and increasing angiogenesis in the dysfunctional diabetic wound microenvironment may be able to accelerate diabetic wound healing.

There are potential limitations to our study. First and foremost, we have targeted CCR10-mediated eNOS downregulation as a key determinant of nonhealing wounds, and we know there are many other cells that respond to CCL28 via CCR10 signaling as well as other mediators that contribute to chronic inflammation associated with nonhealing diabetic skin wounds. Thus, it would be informative to compare the effect of blocking excessive CCL28 signaling via monoclonal neutralizing Ab (thus preventing CCL28 signaling in all responsive cell types in the wound), to the effect of Myr-CBD7 peptide treatment of *db/db* mouse wounds that targets the CCR10/eNOS interaction in ECs. Ideally, this experiment would also be performed in *db/db* mice treated with an eNOS inhibitor or following eNOS depletion to be able to understand the role of eNOS-derived NO production versus inhibition of other CCR10-signaling mechanisms in the anti-inflammatory effects of Myr-CBD7 versus anti-CCL28 Ab. Second, we have not measured the peptide concentration achieved by our topical delivery protocol in vivo (in the wound or circulation) during the first 24 h after skin wounding. Establishing critical pharmacokinetic profiles of Myr-CBD7 and the scrambled control peptide will be important next steps in the development of treatment protocols and for establishing effectiveness and safety profiles prior to first-in-human trials. Third, there are, of course, major differences in wound size, depth, diffusion distances, and the proteolytic environment between mouse and human skin wounds. Nonetheless, we speculate, based on the observed similarities in CCL28 upregulation and CCR10-dependent eNOS downregulation, that topical application of Myr-CBD7 will also stimulate wound healing of human DFUs by enhancing NO bioavailability and thereby reducing inflammation and promoting angiogenesis.

In summary, we established a novel mechanism of CCL28-mediated CCR10-dependent downregulation of eNOS expression in diabetic dermal microvessels. Inhibition of CCR10-eNOS interaction restored eNOS-derived NO production, which normalized inflammation, enhanced angiogenesis, and reduced skin wound healing time in diabetic mice, suggesting this mechanism has the potential to be targeted pharmacologically for treating nonhealing wounds such as DFUs.

**Acknowledgments.** The authors thank Maricela Castellon for technical assistance and management of all animal work, Eileen Brister in the Research Resources Center Research Histology and Tissue Imaging Core, and Peter Toth and Ke Ma in the Research Resources Center Fluorescence Imaging Core for technical support (all at University of Illinois at Chicago). The Myr-CBD7 peptide is protected under U.S. Patent and Trademark Office application number 62879717.

**Funding.** This work was supported in part by National Institutes of Health National Heart, Lung, and Blood Institute grants HL125356 and HL142636 (R.D.M.), National Institute of Diabetes and Digestive and Kidney Diseases grant DK109948 (J.M.H.), and National Institute of General Medical Sciences grant R35GM136228 (T.J.K.); American Diabetes Association grant 1-14-JF-32 (J.M.H.), Clinical and Translational Science Awards program UL1RR029879 sponsored by U54 TR002003 pilot funding (R.D.M., T.J.K., J.M.H.), and the University of Illinois at Chicago Chancellor's Translational Research Initiative (R.D.M., Z.C.).

**Duality of Interest.** No potential conflicts of interest relevant to this article were reported.

**Author Contributions.** Z.C. performed most of the experiments and wrote the first draft of the manuscript. Z.C. and R.D.M. designed the study. J.M.H., L.C., Y.J., and M.S. provided experimental data and technical support. J.M.H., L.C., L.A.D., N.X., S.C.W., T.J.K., and R.D.M. provided critical reagents, participated in discussions, and reviewed and edited the manuscript. Z.C. and R.D.M. are the guarantors of this work and, as such, had full access to all the data in the study and take responsibility for the integrity of the data and the accuracy of the data analysis.

## References

1. Hoffstad O, Mitra N, Walsh J, Margolis DJ. Diabetes, lower-extremity amputation, and death. Diabetes Care 2015;38:1852–1857

2. Boulton AJ. The diabetic foot: from art to science. The 18th Camillo Golgi lecture. Diabetologia 2004;47:1343–1353

3. Walsh JW, Hoffstad OJ, Sullivan MO, Margolis DJ. Association of diabetic foot ulcer and death in a population-based cohort from the United Kingdom. Diabet Med 2016;33:1493–1498

4. Jhamb S, Vangaveti VN, Malabu UH. Genetic and molecular basis of diabetic foot ulcers: clinical review. J Tissue Viability 2016;25:229–236
5. Gallagher KA, Liu ZJ, Xiao M, et al. Diabetic impairments in NO-mediated endothelial progenitor cell mobilization and homing are reversed by hyperoxia and SDF-1 alpha. J Clin Invest 2007;117:1249–1259
6. Liu ZJ, Velazquez OC. Hyperoxia, endothelial progenitor cell mobilization, and diabetic wound healing. Antioxid Redox Signal 2008;10:1869–1882
7. Okonkwo UA, Chen L, Ma D, et al. Compromised angiogenesis and vascular Integrity in impaired diabetic wound healing. PLoS One 2020;15:e0231962
8. Lee PC, Salyapongse AN, Bragdon GA, et al. Impaired wound healing and angiogenesis in eNOS-deficient mice. Am J Physiol 1999;277:H1600–H1608
9. Haberzettl P, McCracken J, Hill BD, Bhatnagar A, Conklin DJ. Abstract 16043: The role of eNOS signaling in wound healing in a murine model of diet-induced obesity. Circulation 2014;130:A16043
10. Han X, Deng Y, Yu J, et al. Acarbose accelerates wound healing via Akt/eNOS signaling in *db/db* mice. Oxid Med Cell Longev 2017;2017:7809581
11. Witte MB, Kiyama T, Barbul A. Nitric oxide enhances experimental wound healing in diabetes. Br J Surg 2002;89:1594–1601
12. Yang Y, Yin D, Wang F, Hou Z, Fang Z. In situ eNOS/NO up-regulation—a simple and effective therapeutic strategy for diabetic skin ulcer. Sci Rep 2016;6:30326
13. Santra S, Rawat A, Pattarayan D, Roy S. Chapter 3 Chronic infection and inflammation: Hallmarks of diabetic foot ulcers. In *Wound Healing, Tissue Repair, and Regeneration in Diabetes*. Bagchi D, Das A, Roy S, Eds. London, Academic Press, 2020, pp. 39 – 47
14. Dinh T, Tecilazich F, Kafanas A, et al. Mechanisms involved in the development and healing of diabetic foot ulceration. Diabetes 2012;61:2937–2947
15. Yin H, Chao L, Chao J. Nitric oxide mediates cardiac protection of tissue kallikrein by reducing inflammation and ventricular remodeling after myocardial ischemia/reperfusion. Life Sci 2008;82:156–165
16. Blais V, Rivest S. Inhibitory action of nitric oxide on circulating tumor necrosis factor-induced NF-kappaB activity and COX-2 transcription in the endothelium of the brain capillaries. J Neuropathol Exp Neurol 2001;60:893–905
17. Grumbach IM, Chen W, Mertens SA, Harrison DG. A negative feedback mechanism involving nitric oxide and nuclear factor kappa-B modulates endothelial nitric oxide synthase transcription. J Mol Cell Cardiol 2005;39:595–603
18. Wang W, Soto H, Oldham ER, et al. Identification of a novel chemokine (CCL28), which binds CCR10 (GPR2). J Biol Chem 2000;275:22313–22323
19. Marchese A, Docherty JM, Nguyen T, et al. Cloning of human genes encoding novel G protein-coupled receptors. Genomics 1994;23:609–618
20. Pan J, Kunkel EJ, Gosslar U, et al. A novel chemokine ligand for CCR10 and CCR3 expressed by epithelial cells in mucosal tissues. J Immunol 2000;165:2943–2949
21. Buskermolen JK, Roffel S, Gibbs S. Stimulation of oral fibroblast chemokine receptors identifies CCR3 and CCR4 as potential wound healing targets. J Cell Physiol 2017;232:2996–3005
22. Facciabene A, Peng X, Hagemann IS, et al. Tumour hypoxia promotes tolerance and angiogenesis via CCL28 and T(reg) cells. Nature 2011;475:226–230
23. Bünemann E, Hoff NP, Buhren BA, et al. Chemokine ligand-receptor interactions critically regulate cutaneous wound healing. Eur J Med Res 2018;23:4
24. Chen Z, Kim SJ, Essani AB, et al. Characterising the expression and function of CCL28 and its corresponding receptor, CCR10, in RA pathogenesis. Ann Rheum Dis 2015;74:1898–1906
25. Chen Z, Haus JM, Chen L, et al. CCL28-induced CCR10/eNOS interaction in angiogenesis and skin wound healing. FASEB J 2020;34:5838–5850
26. Mahmoud AM, Szczurek MR, Blackburn BK, et al. Hyperinsulinemia augments endothelin-1 protein expression and impairs vasodilation of human skeletal muscle arterioles. Physiol Rep 2016;4:e12895
27. Mey JT, Blackburn BK, Miranda ER, et al. Dicarbonyl stress and glyoxalase enzyme system regulation in human skeletal muscle. Am J Physiol Regul Integr Comp Physiol 2018;314:R181–R190
28. Chen Z, D S Oliveira S, Zimnicka AM, et al. Reciprocal regulation of eNOS and caveolin-1 functions in endothelial cells. Mol Biol Cell 2018;29:1190–1202
29. Mirza R, DiPietro LA, Koh TJ. Selective and specific macrophage ablation is detrimental to wound healing in mice. Am J Pathol 2009;175:2454–2462
30. Zhao Y, Bao L, Chan LS, DiPietro LA, Chen L. Aberrant wound healing in an epidermal interleukin-4 transgenic mouse model of atopic dermatitis. PLoS One 2016;11:e0146451
31. Chen Z, Bakhshi FR, Shajahan AN, et al. Nitric oxide-dependent Src activation and resultant caveolin-1 phosphorylation promote eNOS/caveolin-1 binding and eNOS inhibition. Mol Biol Cell 2012;23:1388–1398
32. Chen Z, Kim SJ, Chamberlain ND, et al. The novel role of IL-7 ligation to IL-7 receptor in myeloid cells of rheumatoid arthritis and collagen-induced arthritis. J Immunol 2013;190:5256–5266
33. Das A, Ghatak S, Sinha M, et al. Correction of MFG-E8 resolves inflammation and promotes cutaneous wound healing in diabetes. J Immunol 2016;196:5089–5100
34. Singh K, Sinha M, Pal D, et al. Cutaneous epithelial to mesenchymal transition activator ZEB1 regulates wound angiogenesis and closure in a glycemic status-dependent manner. Diabetes 2019;68:2175–2190
35. Charakida M, Masi S, Lüscher TF, Kastelein JJ, Deanfield JE. Assessment of atherosclerosis: the role of flow-mediated dilatation. Eur Heart J 2010;31:2854–2861
36. Homey B, Wang W, Soto H, et al. Cutting edge: the orphan chemokine receptor G protein-coupled receptor-2 (GPR-2, CCR10) binds the skin-associated chemokine CCL27 (CTACK/ALP/ILC). J Immunol 2000;164:3465–3470
37. Balkwill F. Cancer and the chemokine network. Nat Rev Cancer 2004;4:540–550
38. Kroeze KL, Boink MA, Sampat-Sardjoepersad SC, Waaijman T, Scheper RJ, Gibbs S. Autocrine regulation of re-epithelialization after wounding by chemokine receptors CCR1, CCR10, CXCR1, CXCR2, and CXCR3. J Invest Dermatol 2012;132:216–225
39. Calebiro D, Nikolaev VO, Persani L, Lohse MJ. Signaling by internalized G-protein-coupled receptors. Trends Pharmacol Sci 2010;31:221–228
40. Sussman C. Management of wound healing with biophysical agent technologies. In *Wound Care: A Collaborative Practice Manual for Health Professionals*. 3rd ed. Sussman C, Bates-Jensen B, Eds. Baltimore, Lippincott Williams & Wilkins, 2007, p. 498
41. Förstermann U, Münzel T. Endothelial nitric oxide synthase in vascular disease: from marvel to menace. Circulation 2006;113:1708–1714
42. Candido R, Bernardi S, Allen TJ. Linking diabetes and atherosclerosis. Expert Rev Endocrinol Metab 2009;4:603–624
43. Ceriello A. Point: postprandial glucose levels are a clinically important treatment target. Diabetes Care 2010;33:1905–1907
44. Walton DM, Minton SD, Cook AD. The potential of transdermal nitric oxide treatment for diabetic peripheral neuropathy and diabetic foot ulcers. Diabetes Metab Syndr 2019;13:3053–3056
45. Jeffcoate WJ, Harding KG. Diabetic foot ulcers. Lancet 2003;361:1545–1551
46. El-Mesallamy HO, Hamdy NM, Ezzat OA, Reda AM. Levels of soluble advanced glycation end product-receptors and other soluble serum markers as indicators of diabetic neuropathy in the foot. J Investig Med 2011;59:1233–1238
47. Hu S, Yang K, Yang J, Li M, Xiong N. Critical roles of chemokine receptor CCR10 in regulating memory IgA responses in intestines. Proc Natl Acad Sci U S A 2011;108:E1035–E1044
48. Duplain H, Burcelin R, Sartori C, et al. Insulin resistance, hyperlipidemia, and hypertension in mice lacking endothelial nitric oxide synthase. Circulation 2001;104:342–345
49. Frank S, Kämpfer H, Wetzler C, Pfeilschifter J. Nitric oxide drives skin repair: novel functions of an established mediator. Kidney Int 2002;61:882–888
50. Rajendran S, Shen X, Glawe J, Kolluru GK, Kevil CG. Nitric oxide and hydrogen sulfide regulation of ischemic vascular growth and remodeling. Compr Physiol 2019;9:1213–1247

51. Yuan S, Kevil CG. Nitric oxide and hydrogen sulfide regulation of ischemic vascular remodeling. Microcirculation 2016;23:134–145
52. Luo JD, Chen AF. Nitric oxide: a newly discovered function on wound healing. Acta Pharmacol Sin 2005;26:259–264
53. Jozkowicz A, Cooke JP, Guevara I, et al. Genetic augmentation of nitric oxide synthase increases the vascular generation of VEGF. Cardiovasc Res 2001;51:773–783
54. Dulak J, Józkowicz A, Dembinska-Kiec A, et al. Nitric oxide induces the synthesis of vascular endothelial growth factor by rat vascular smooth muscle cells. Arterioscler Thromb Vasc Biol 2000;20:659–666
55. Wietecha MS, DiPietro LA. Therapeutic approaches to the regulation of wound angiogenesis. Adv Wound Care (New Rochelle) 2013;2:81–86
56. Caviedes A, Maturana B, Corvalán K, et al. eNOS-dependent S-nitrosylation of the NF-κB subunit p65 has neuroprotective effects. Cell Death Dis 2021;12:4
57. Póvoa VCO, Dos Santos GJVP, Picheth GF, et al. Wound healing action of nitric oxide-releasing self-expandable collagen sponge. J Tissue Eng Regen Med 2020;14:807–818
58. Witte MB, Thornton FJ, Efron DT, Barbul A. Enhancement of fibroblast collagen synthesis by nitric oxide. Nitric Oxide 2000;4:572–582